Monthly Notices of the ROYAL ASTRONOMICAL SOCIETY

MNRASL **438,** L76–L80 (2014) doi:10.1093/mnrasl/slt162
Advance Access publication 2013 December 9

From solar-like to antisolar differential rotation in cool stars

T. Gastine,[1⋆] R. K. Yadav,[1,2] J. Morin,[2,3] A. Reiners[2] and J. Wicht[1]

[1]*Max Planck Institut für Sonnensystemforschung, Max-Planck Strasse 2., D-37191 Katlenburg-Lindau, Germany*
[2]*Institut für Astrophysik, Georg-August-Universität Göttingen, Friedrich-Hund Platz, D-37077 Göttingen, Germany*
[3]*LUPM–UMR5299, CNRS & Université Montpellier II, Place E. Bataillon, F-34095 Montpellier Cedex 05, France*

Accepted 2013 November 8. Received 2013 November 5; in original form 2013 October 10

ABSTRACT

Stellar differential rotation can be separated into two main regimes: solar-like when the equator rotates faster than the poles and antisolar when the polar regions rotate faster than the equator. We investigate the transition between these two regimes with 3D numerical simulations of rotating spherical shells. We conduct a systematic parameter study which also includes models from different research groups. We find that the direction of the differential rotation is governed by the contribution of the Coriolis force in the force balance, independently of the model setup (presence of a magnetic field, thickness of the convective layer, density stratification). Rapidly rotating cases with a small Rossby number yield solar-like differential rotation, while weakly rotating models sustain antisolar differential rotation. Close to the transition, the two kinds of differential rotation are two possible bistable states. This study provides theoretical support for the existence of antisolar differential rotation in cool stars with large Rossby numbers.

Key words: convection – MHD – turbulence – Sun: rotation – stars: rotation.

1 INTRODUCTION

The solar surface rotates differentially with the equatorial regions rotating faster than the poles. In addition, helioseismic measurements revealed the internal rotation profile of the Sun: (i) the outer convective region exhibits significant latitudinal gradients of shear; (ii) a strong radial differential rotation is observed at the bottom of the convective zone forming the tachocline; (iii) and the radiative core rotates nearly uniformly (e.g. Thompson et al. 2003).

In cool stars other than the Sun, the surface differential rotation can be inferred from different measurements techniques encompassing Doppler imaging (e.g. Collier Cameron, Donati & Semel 2002), Fourier transform of the spectral lines (e.g. Reiners & Schmitt 2002) or period detection in the photometric measurements (e.g. Reinhold, Reiners & Basri 2013). The latitudinal differential rotation in stars is usually described by a single-parameter law of the form $\Omega(\theta) = \Omega_e(1 - \alpha \sin^2\theta)$, θ being the latitude and Ω_e the angular velocity at the equator. Differential rotation is then usually categorized as 'solar-like' when $\alpha > 0$ ($\alpha_\odot = 0.2$), or as 'antisolar' when the polar regions rotate faster than the equator (i.e. $\alpha < 0$). For main- and pre-main-sequence stars, observations of absolute surface shear show some dependence on rotation period and effective temperature (Barnes et al. 2005; Ammler-von Eiff & Reiners 2012; Reinhold et al. 2013). Information on the sign of differential rotation is very sparse because observational signatures are very subtle (Fourier technique) or only the absolute value is obtained (photometric technique). Up to now, antisolar differential rotation has only been reported for a handful of K giant stars observed with the Doppler imaging technique (e.g. Strassmeier, Kratzwald & Weber 2003; Weber, Strassmeier & Washuettl 2005; Kovári et al. 2007). We may thus wonder what determines the sign of differential rotation in cool stars.

The first theoretical approach to model stellar differential rotation relies on hydrodynamical mean-field models (e.g. Ruediger 1989). In a similar way as in the mean-field dynamo models, the velocity components u_i are therefore decomposed into a mean-field contribution $\bar{u}_i$ and in a fluctuating part u_i'. The quadratic correlations of the fluctuating quantities, such as Reynolds stresses $\mathcal{Q}_{ij} = \overline{u_i' u_j'}$, are then parametrized as functions of the mean-field quantities only. Reynolds stresses are for instance expanded assuming $\mathcal{Q}_{ij} = \Lambda_{ijk}\bar{\Omega}_k - N_{ijkl}\partial\bar{u}_k/\partial x_l$, where Λ_{ijk} and N_{ijkl} are third- and fourth-order tensors, respectively. The parametrization of the velocity correlations $\mathcal{Q}_{ij}$ thus involves some free coefficients (turbulent viscosity for instance) that need to be set to ensure the closure of the mean-field model. Despite these approximations, mean-field approaches were quite successful in predicting a weak dependence of the surface shear on the rotation rate and a strong correlation with the effective temperature as observed on the main-sequence stars (Küker & Rüdiger 2011). In addition, these models have a strong prediction concerning the sense of the differential rotation and predominantly yield solar-like $\Omega(\theta)$ profiles (Kitchatinov & Rüdiger 1999). Antisolar differential rotation can only be maintained in the case of very strong meridional circulation (Kitchatinov & Rüdiger 2004).

Alternatively, stellar differential rotation can be modelled using 3D hydrodynamical and dynamo models of rotating convection in spherical geometry. In that case, the differential rotation is

⋆E-mail: gastine@mps.mpg.de

maintained by the interaction of turbulent convection with rotation. Despite their own limitations (high diffusivities and moderate density contrasts), 3D models allow us to fully take into account the non-linearities involved in the angular momentum transport. In contrast with mean-field approaches, no parametrization of Reynolds stresses is required in 3D simulations. Although a large number of such simulations yield solar-like differential rotation, they have also frequently produced antisolar differential rotation over a broad range of parameters and model setups (e.g. Gilman 1977; Glatzmaier & Gilman 1982; Aurnou, Heimpel & Wicht 2007; Steffen & Freytag 2007; Bessolaz & Brun 2011; Käpylä et al. 2011; Matt et al. 2011; Gastine, Wicht & Aurnou 2013a, hereafter GWA13). The differential rotation direction is suspected to be controlled by the relative contribution of buoyancy and Coriolis force in the global force balance (Gilman 1977; Aurnou et al. 2007). Cases where rotation dominates the force balance yield prograde equatorial azimuthal flows, while a weak rotational influence leads to antisolar differential rotation. As shown in previous parameter studies, these two regimes can be well separated by a critical convective Rossby number of unity (Gilman 1977), independently of the background density stratification (Gastine & Wicht 2012, hereafter GW12; GWA13).

This work extends these studies to a broader range of parameters to investigate the zonal flow transition in 3D models in a systematic way. For the sake of generality, we also incorporate data of different research groups who reported antisolar differential rotation in their models.

2 HYDRODYNAMICAL MODEL

We consider numerical simulations of an anelastic ideal gas in spherical shells rotating at a constant rotation rate Ω_0. A fixed entropy contrast Δs between the inner and the outer boundary drives the convective motions. Our numerical models are computed using the anelastic spectral code MAGIC (Wicht 2002; GW12) that has been validated against hydrodynamical and dynamo benchmarks (Jones et al. 2011). We non-dimensionalize the MHD equations using Ω_0^{-1} as the time unit and the shell thickness $d = r_\mathrm{o} - r_\mathrm{i}$ as the reference length-scale. The anelastic system of equations is then governed by four dimensionless parameters

$$E = \frac{\nu}{\Omega_0 d^2}, \quad Ra = \frac{g_\mathrm{o} d^3 \Delta s}{c_p \nu \kappa}, \quad Pr = \frac{\nu}{\kappa}, \quad Pm = \frac{\nu}{\lambda}, \tag{1}$$

where ν, κ and λ are the constant kinematic, thermal and magnetic diffusivities and g_o is the gravity at the outer boundary. Details of the numerical implementation are extensively discussed by Jones et al. (2011) and GW12. Differential rotation maintained in 3D models is suspected to be sensitive to the relative contribution of buoyancy and Coriolis force in the force balance. The ratio between these two forces can be roughly assessed by the so-called *convective Rossby number*, defined by $Ro_\mathrm{c} = \sqrt{Ra\, E^2/Pr}$.

The converged solution of a numerical simulation is then characterized by several diagnostic parameters. The rms flow velocity is given in units of the Rossby number $Ro' = u'_\mathrm{rms}/\Omega_0 d$, where primed quantities correspond to the non-axisymmetric contribution. The typical flow length-scale ℓ is defined as $\ell = \pi d/\bar{l}_u$, where $\bar{l}_u$ is the mean spherical harmonic degree obtained from the kinetic energy spectrum (e.g. Christensen & Aubert 2006; Schrinner, Petitdemange & Dormy 2012). A *local Rossby number* $Ro_\ell = u'_\mathrm{rms}/\Omega_0 \ell$ can then be used to evaluate the relative contribution of inertia and Coriolis force to the global force balance. Differential rotation is quantified by the amplitude of the equatorial surface zonal flow

$$\alpha_\mathrm{e} = \frac{\bar{u}_\phi(r = r_\mathrm{o}, \theta = 0)}{\Omega_\mathrm{o} r_\mathrm{o}} = \frac{\mathrm{d}\Omega(r = r_\mathrm{o}, \theta = 0)}{\Omega_\mathrm{o}}, \tag{2}$$

where overbars denote axisymmetric quantities.

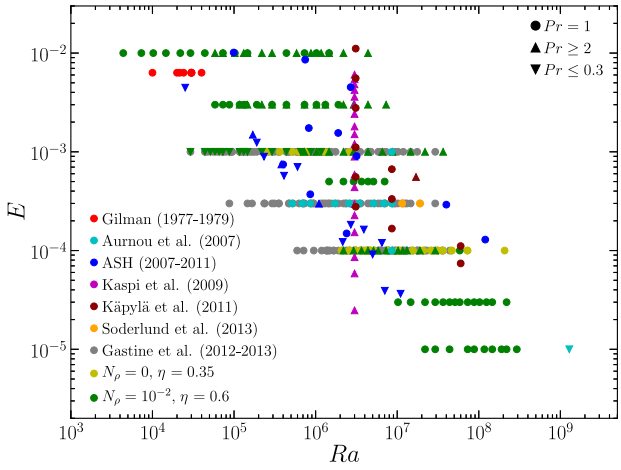

Figure 1. Dimensionless control parameters explored by various numerical models computed with different codes. Data have been gathered and adapted from Gilman (1977, 1979), Aurnou et al. (2007), ASH (Ballot, Brun & Turck-Chièze 2007; Browning 2008; Brown 2009; Brun & Palacios 2009; Matt et al. 2011; Bessolaz & Brun 2011), Kaspi, Flierl & Showman (2009), Käpylä et al. (2011), Soderlund et al. (2013); GW12 and GWA13.

Our previous parameter studies were dedicated to the effects of the density stratification on the differential rotation (GW12; GWA13). They assumed $Pr = 1$ and covered a limited range of Ekman numbers ($E = 10^{-3} - 10^{-4}$). To extend the coverage of the parameter space, we have computed here 150 new cases which span the range of $10^{-5} < E < 10^{-2}$, $10^3 < Ra < 5 \times 10^8$ and $Pr \in [0.1, 1, 10]$. We consider here non-magnetic nearly Boussinesq models (i.e. $N_\rho = \ln(\rho_\mathrm{bot}/\rho_\mathrm{top}) = 10^{-2}$) in a thin spherical shell of aspect ratio $\eta = r_\mathrm{i}/r_\mathrm{o} = 0.6$. To investigate how the magnetic field influences differential rotation, we also consider a few Boussinesq dynamo models with $\eta = 0.35$ and $Pm = 1$.

Furthermore, we include additional data from published studies which encompasses Boussinesq (e.g. Aurnou et al. 2007), anelastic spherical harmonic (ASH; e.g. Gilman 1977) and fully compressible 3D models (Käpylä et al. 2011). To our knowledge, all the data reporting antisolar differential rotation have been gathered in Fig. 1, provided control and relevant diagnostic parameters (i.e. α_e) were accessible. Note that to ease the comparison between the different setups, the Rayleigh numbers have been rescaled in Fig. 1 to use the entropy gradient at mid-depth, i.e. $Ra = g_\mathrm{o} d^3 |ds/dr|_m / c_p \nu \kappa$. This provides a better way of comparing different reference state models (see Kaspi et al. 2009; GWA13).

3 RESULTS

3.1 Differential rotation regimes

Fig. 2 shows the surface differential rotation amplitude α_e as a function of Ro_c for the Fig. 1 data set. When Coriolis forces dominate the force balance (i.e. $Ro_\mathrm{c} \ll 1$, regime I), the equatorial zonal flow is prograde and its amplitude increases with Ro_c. A relatively sharp transition to retrograde zonal winds (or antisolar differential

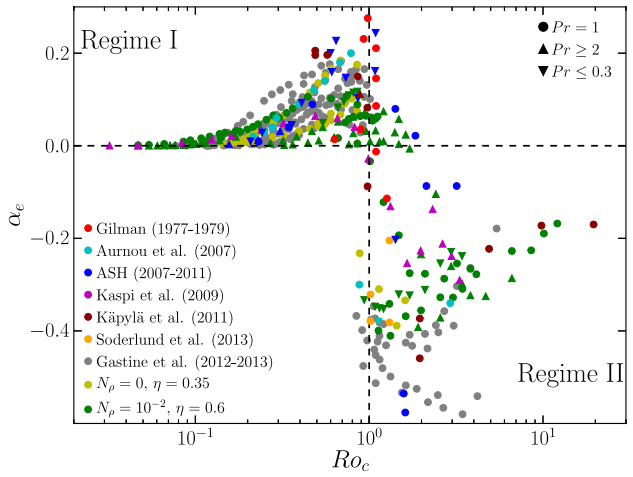

Figure 2. Amplitude of the surface zonal flows at the equator in units of $\alpha_e = \bar{u}_\phi / \Omega_0 r_o$ as a function of Ro_c for the numerical models of Fig. 1.

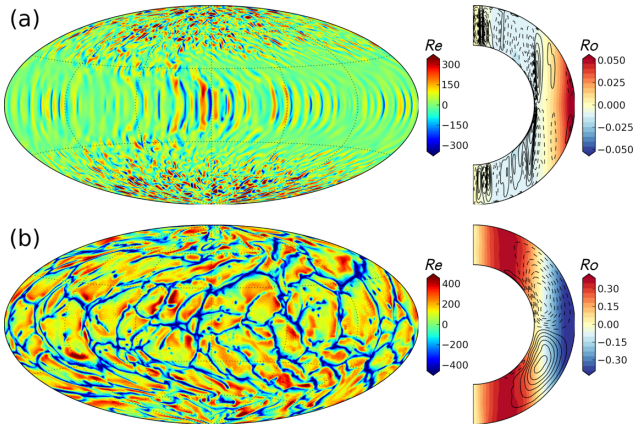

Figure 3. Left-hand panels: radial velocity at $r = 0.95\, r_o$. Right-hand panels: time-averaged zonal velocity (coloured levels) and meridional circulation (solid and dashed lines). Case (a) corresponds to $N_\rho = 3$, $\eta = 0.6$, $E = 10^{-4}$, $Ra = 9 \times 10^6$, $Pr = 1$, case (b) to $N_\rho = 3$, $\eta = 0.6$, $E = 10^{-3}$, $Ra = 4 \times 10^6$, $Pr = 1$. Radial velocity is given in Reynolds number units ($u_r d/\nu$) while zonal flows are expressed in Rossby number units.

rotation) then occurs close to $Ro_c \sim 1$. Although the data set is scattered, the retrograde equatorial flow is on average stronger than in regime I and reaches values of $\alpha_e \sim -0.4$ for $Ro_c \sim 1$. When buoyancy starts to dominate the force balance (i.e. $Ro_c \gg 1$, regime II), the differential rotation decreases suggesting a possible third regime where turbulent motion gradually suppress the mean flows ($Ro_c > 10$, see GWA13 and Brummell, Hurlburt & Toomre 1998).

Despite differences in size of the convective layer, values of the control parameters, definition of the Rayleigh number, choice of thermal boundary conditions and so on, the transition between regimes I and II is well captured by Ro_c, with all the data points concentrating in the top-left and bottom-right quadrants.

To illustrate the differences in the differential rotation patterns in the two regimes, Fig. 3 shows radial velocity and zonal flows for two selected models. In the rotation-dominated regime ($Ro_c = 0.09$, upper panels) convective columns aligned with the rotation axis are visible at low latitudes. They are accompanied at higher latitudes by small-scale time-dependent convective cells. Due to the curvature of the spherical shell, the convective columns are slightly tilted in the prograde direction and give rise to Reynolds stresses (a statistical correlation between the convective flow components, see Busse 1983; Christensen 2002). Reynolds stresses maintain a positive flux of angular momentum away from the rotation axis which is responsible for the observed differential rotation. The pair of geostrophic zonal flows with an eastward equator and westward poles is typical in this regime (e.g. Käpylä et al. 2011; GW12). In contrast, when buoyancy becomes a first-order contribution in the force balance ($Ro_c = 4$, lower panels), the convective features lose their preferred alignment with the rotation axis and the zonal flow direction reverses. The equatorial jet becomes retrograde and is flanked by two prograde zonal winds inside the tangent cylinder. The antisolar differential rotation observed here can be attributed to the mixing of angular momentum by the turbulent convective motions (e.g. Gilman & Foukal 1979; Aurnou et al. 2007). As demonstrated by GWA13, the angular momentum per unit mass $\mathcal{M}$ is thus a conserved quantity such that

$$\mathcal{M} = \bar{u}_\phi s + \Omega_0\, s^2 = \text{const.} = \zeta(\eta, N_\rho)\Omega_0 r_o^2, \tag{3}$$

where s is the cylindrical radius and $0 < \zeta(\eta, N_\rho) < 1$ depends on the background density stratification, the size of the convective zone and the efficiency of the angular momentum mixing. Using $\Omega_0 r_o^2$ to non-dimensionalize this equation leads to the following formulation of the differential rotation in regime II:

$$Ro = \frac{\bar{u}_\phi}{\Omega_0 r_o} = \zeta(\eta, N_\rho)\frac{r_o}{s} - \frac{s}{r_o}. \tag{4}$$

Comparisons between the zonal flow profiles and this theoretical prediction give good agreement for models with $Ro_c \gtrsim 1$ (Aurnou et al. 2007; GWA13).

Meridional circulation patterns change when differential rotation changes sign (e.g. Bessolaz & Brun 2011; Matt et al. 2011). In the upper panel of Fig. 3, multiple small-scale meridional circulation cells are observed, while the second model shows only one large-scale cell in each hemisphere. This transition results from a change in the spatial variations of the azimuthal force balance between viscous and Reynolds stresses (a mechanism sometimes known as 'gyroscopic pumping', e.g. Miesch & Hindman 2011).

Fig. 4(a) shows the same quantities as Fig. 2 for a consistent subset of nearly Boussinesq numerical models ($N_\rho = 10^{-2}$) with $\eta = 0.6$. This subset is partly composed by the Boussinesq models of GW12 and GWA13 and partly by the additional cases computed for the present study. Considering the same reference model for the whole subset allows us to more accurately scrutinize the zonal flow transition. While the regime change occurs in the range $0.8 < Ro_c < 2$, some parameter dependence is still noticeable. For instance, the transition is rather gradual for large Ekman numbers ($E = 10^{-2}$, magenta symbols) and becomes sharper when the Ekman number is lowered. Moreover, the Prandtl number dependence does not seem to be perfectly captured by Ro_c. In fact, the zonal flow transition in the numerical models with $Pr = 10$ ($Pr = 0.1$) takes place at higher (lower) values of Ro_c than the $Pr = 1$ cases. As our data set is limited to relatively large Ekman numbers for $Pr \neq 1$, we might however speculate that such Pr dependence vanishes at low Ekman numbers. As shown in Fig. 4(b), the zonal flow transition is better captured when α_e is plotted against the local Rossby number Ro_ℓ. This reduction of the dispersion is expected as Ro_c is only a rough proxy of the convective Rossby number, while Ro_ℓ is a measure of the actual local Rossby number of a numerical model. A precise estimate of Ro_ℓ for the whole data set of models shown in Fig. 2 would thus also help to reduce the observed dispersion.

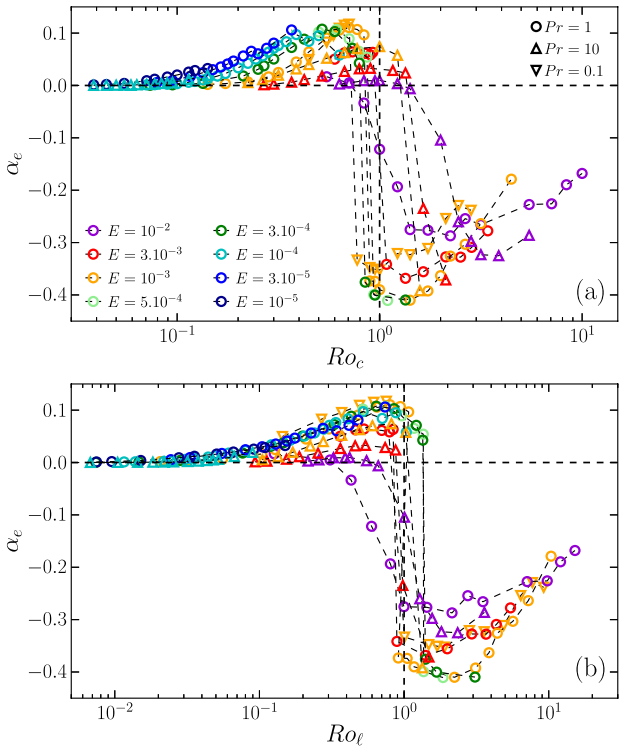

Figure 4. (a) α_e as a function of Ro_c and (b) as a function of Ro_ℓ. All the numerical models have $N_\rho = 10^{-2}$ and $\eta = 0.6$.

3.2 Zonal flow bistability

We find several cases of bistability where the two kinds of differential rotation are stable at identical parameters (i.e. Ra, E and Pr) when $Ro_c \sim Ro_\ell \sim 1$. The initial condition then selects which differential rotation profile will be adopted by the converged solution. As shown in Fig. 5, starting from a model with a solar-like differential rotation and increasing Ro_c (or Ro_ℓ) maintains a solution with the same kind of differential rotation for $0.5 < Ro_\ell < 1.3$ before falling on the other branch at higher Ro_ℓ. Alternatively, if one initiates this model with $\alpha_e < 0$ and decreases Ro_c, the solution may remain on that branch. Once again, the Pr dependence on the bistability region seems to be better captured when one considers Ro_ℓ instead of Ro_c. The hysteresis loop is relatively narrow for $E = 10^{-3}$ and becomes wider at $E = 3 \times 10^{-4}$. At $E = 10^{-4}$, it becomes numerically too demanding to further investigate the extent of the two branches. Hence, an Ekman number dependence cannot be completely ruled out and the extent of the bistability region might increase further when E is lowered.

3.3 Magnetic field influence

To investigate if the zonal flow transition is affected by the presence of magnetic field, we compute two sets of Boussinesq models with $\eta = 0.35$: one consists of non-magnetic cases, while the other contains their dynamo counterparts. Fig. 6 shows that in both cases the transition between regimes I and II occurs around $Ro_\ell \sim 1$. Due to the influence of the magnetic field on the convective flow velocity and length-scale, the exact value of Ro_ℓ at the transition is slightly lower in the dynamo models. In the rotation-dominated regime, the magnetic cases have significantly weaker zonal flows than the non-magnetic ones. In contrast, hydrodynamical and dynamo models yield similar zonal flow amplitude in regime II, confirming the previous findings by Soderlund et al. (2013). These differences can be attributed to the relative efficiency of the magnetic braking. The quenching of the differential rotation by Lorentz forces is indeed more pronounced when the magnetic field has a significant large-scale contribution ($Ro_\ell < 1$; Yadav, Gastine & Christensen 2013).

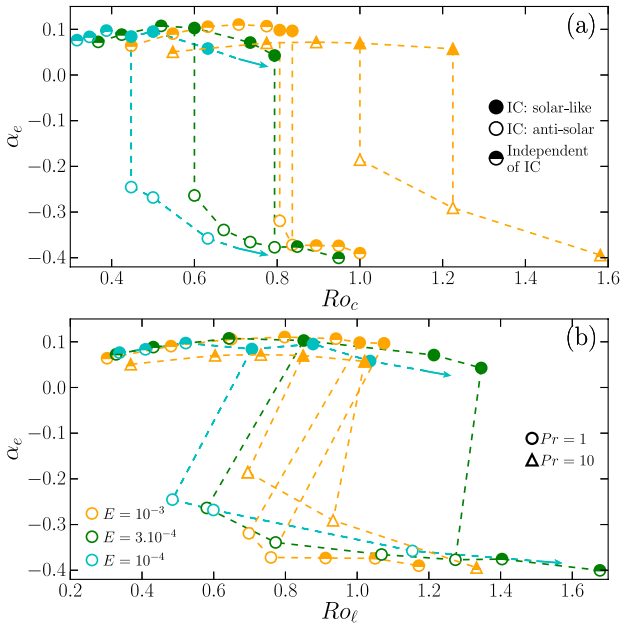

Figure 5. (a) α_e as a function of Ro_c and (b) as a function of Ro_ℓ. Selection of numerical models with $N_\rho = 10^{-2}$ and $\eta = 0.6$ to illustrate the bistability of the zonal flow. The dependence on the initial conditions (IC) is shown by different symbol fill styles. The blue arrows indicate possible continuation of the hysteresis loop for the $E = 10^{-4}$ cases.

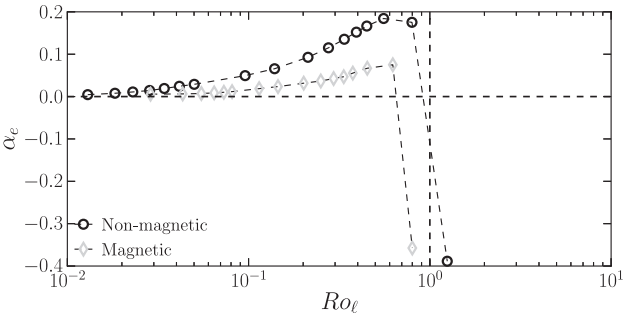

Figure 6. α_e as a function of Ro_ℓ for non-magnetic and magnetic ($Pm = 1$) models with $N_\rho = 0$, $\eta = 0.35$, $E = 10^{-4}$ and $Pr = 1$.

4 DISCUSSION

We investigate the transition between solar-like and antisolar differential rotation in rotating spherical shells. We extend previous studies (GW12; GWA13) with a new set of models which covers a broader range of control parameters. We also include models published by various groups in our analysis.

From this set of simulations, we confirm previous findings that the direction of differential rotation is determined by the value of the convective Rossby number defined as $Ro_c = \sqrt{Ra\,E^2/Pr}$. In the rotation-dominated regime (regime I, $Ro_c < 1$), the differential rotation is solar-like, i.e. the equator rotates faster than the

poles. When buoyancy dominates the force balance ($Ro_c > 1$), the turbulent convective motions homogenize the angular momentum, which leads to antisolar differential rotation profiles. The regime transition takes place at $Ro_c \sim 1$, independently of the details of the model (density stratification, thickness of the convective layer and so on). We show that the local Rossby number Ro_ℓ – a good proxy of the relative contribution of Coriolis force and inertia in the force balance (Christensen & Aubert 2006) – helps to better separate the two regimes. Close to the transition ($0.5 < Ro_\ell < 1.5$), the two kinds of differential rotation are two possible stable states at the same parameter values, forming a bistable region. The presence of a magnetic field reduces the amplitude of differential rotation in regime I without affecting the regime change at $Ro_\ell \sim 1$.

It should be however noted that global numerical models always operate in a parameter regime far from the stellar values due to their large diffusivities (i.e. small Rayleigh and large Ekman numbers). Hence, the existence of additional dynamical regimes cannot be ruled out at realistic parameters. Nonetheless, antisolar differential rotation is systematically found in weakly rotating 3D simulations in contrast with the mean-field results. A closer comparison between mean-field predictions and 3D simulations is therefore desirable to better establish the limits of validity of such mean-field approaches (e.g. Käpylä et al. 2011).

Our results provide theoretical support for the existence of slowly rotating cool stars exhibiting antisolar differential rotation. A further validation of our prediction requires to estimate Ro_ℓ in stellar convective zones. We adopt $Ro_{\rm emp}$, the ratio of the rotation period $P_{\rm rot}$ and the turnover time of convection $\tau_{\rm conv}$, as our best available proxy for Ro_ℓ (e.g. Gastine et al. 2013b). With $P_{\rm rot} = 25$ d and $\tau_{\rm conv} = 12-50$ d (Reiners 2012), the solar Rossby number lies in the range $0.5 < Ro_{\rm emp} < 2$. This suggests that the Sun might be at the limit of the rotation-dominated regime and that stars with Rossby number just above the solar value could exhibit strong antisolar differential rotation. Claims of antisolar differential rotation are so far restricted to K giants. Most of these stars are in binary systems where tidal effects likely have an impact on the surface shear (e.g. Kovári et al. 2007). The K giant HD 31993 is the only single giant for which a significant antisolar differential rotation is reported ($\alpha = -0.125$; Strassmeier et al. 2003). For this star $P_{\rm rot} = 25.3$ d and $\tau_{\rm conv} \simeq 25$ d (Gunn, Mitrou & Doyle 1998) yield $Ro_{\rm emp} \simeq 1$, a value close to the threshold but compatible with $\alpha < 0$.

Measuring differential rotation for stars clearly in the $Ro > 1$ regime remains challenging. Doppler imaging or line profile analysis are sensitive to the sign of differential rotation but suffer from some limitations. Doppler imaging indeed relies on the presence of large spots at the stellar photosphere which is not expected for $Ro_{\rm emp} > 1$. Line profile analysis requires a minimum rotational velocity $v \sin i_{\rm min} \sim 10-20$ km s^{-1}. This is incompatible with $Ro_{\rm emp} > 1$ for cool main-sequence stars. Although Ammler-von Eiff & Reiners (2012) observed line profile shapes attributable to $\alpha \lesssim 0$ for dwarf stars with $Ro_{\rm emp} < 1$, they attributed these signatures to the presence of cool polar spots. With their larger radii, weakly active evolved giant stars might be more suitable targets. Space missions *CoRoT* and *Kepler* collect high-precision photometric data for a vast sample of stars. Although this technique cannot directly determine the sign of α, a regime change in the differential rotation might still be captured. Our numerical models indeed suggest a relatively sharp rise in $|\alpha|$ at the transition between solar and antisolar differential rotation. Latest results based on moderate to fast rotators ($P_{\rm rot} < 45$ d) by Reinhold et al. (2013) suggest a possible increase of $|\alpha|$ with the Rossby number stressing the need for further analysis of slowly rotating Kepler stars.

ACKNOWLEDGEMENTS

We thank P. Käpylä for providing us the parameters of his numerical models and A. S. Brun for fruitful discussion. Computations have been carried out on the GWDG computer facilities in Göttingen and on HRLN in Hannover. We acknowledge funding from the Deutsche Forschungsgemeinschaft (DFG) through Project SFB 963/A17 and through the Special Priority Program 1488.

REFERENCES

Ammler-von Eiff M., Reiners A., 2012, A&A, 542, A116
Aurnou J., Heimpel M., Wicht J., 2007, Icarus, 190, 110
Ballot J., Brun A. S., Turck-Chièze S., 2007, ApJ, 669, 1190
Barnes J. R., Collier Cameron A., Donati J.-F., James D. J., Marsden S. C., Petit P., 2005, MNRAS, 357, L1
Bessolaz N., Brun A. S., 2011, ApJ, 728, 115
Brown B. P., 2009, PhD thesis, Univ. Colorado
Browning M. K., 2008, ApJ, 676, 1262
Brummell N. H., Hurlburt N. E., Toomre J., 1998, ApJ, 493, 955
Brun A. S., Palacios A., 2009, ApJ, 702, 1078
Busse F. H., 1983, Geophys. Astrophys. Fluid Dyn., 23, 153
Christensen U. R., 2002, J. Fluid Mech., 470, 115
Christensen U. R., Aubert J., 2006, Geophys. J. Int., 166, 97
Collier Cameron A., Donati J.-F., Semel M., 2002, MNRAS, 330, 699
Gastine T., Wicht J., 2012, Icarus, 219, 428 (GW12)
Gastine T., Wicht J., Aurnou J. M., 2013a, Icarus, 225, 156 (GWA13)
Gastine T., Morin J., Duarte L., Reiners A., Christensen U. R., Wicht J., 2013b, A&A, 549, L5
Gilman P. A., 1977, Geophys. Astrophys. Fluid Dyn., 8, 93
Gilman P. A., 1979, ApJ, 231, 284
Gilman P. A., Foukal P. V., 1979, ApJ, 229, 1179
Glatzmaier G. A., Gilman P. A., 1982, ApJ, 256, 316
Gunn A. G., Mitrou C. K., Doyle J. G., 1998, MNRAS, 296, 150
Jones C. A., Boronski P., Brun A. S., Glatzmaier G. A., Gastine T., Miesch M. S., Wicht J., 2011, Icarus, 216, 120
Käpylä P. J., Mantere M. J., Guerrero G., Brandenburg A., Chatterjee P., 2011, A&A, 531, A162
Kaspi Y., Flierl G. R., Showman A. P., 2009, Icarus, 202, 525
Kitchatinov L. L., Rüdiger G., 1999, A&A, 344, 911
Kitchatinov L. L., Rüdiger G., 2004, Astron. Nachr., 325, 496
Kovári Z., Bartus J., Strassmeier K. G., Vida K., Švanda M., Oláh K., 2007, A&A, 474, 165
Küker M., Rüdiger G., 2011, Astron. Nachr., 332, 933
Matt S. P., Do Cao O., Brown B. P., Brun A. S., 2011, Astron. Nachr., 332, 897
Miesch M. S., Hindman B. W., 2011, ApJ, 743, 79
Reiners A., 2012, Living Rev. Sol. Phys., 9, 1
Reiners A., Schmitt J. H. M. M., 2002, A&A, 384, 155
Reinhold T., Reiners A., Basri G., 2013, A&A, in press, doi:10.1051/0004-6361/201321970
Ruediger G., 1989, Differential Rotation and Stellar Convection. Sun and the Solar Stars. Akademie Verlag, Berlin
Schrinner M., Petitdemange L., Dormy E., 2012, ApJ, 752, 121
Soderlund K. M., Heimpel M. H., King E. M., Aurnou J. M., 2013, Icarus, 224, 97
Steffen M., Freytag B., 2007, Astron. Nachr., 328, 1054
Strassmeier K. G., Kratzwald L., Weber M., 2003, A&A, 408, 1103
Thompson M. J., Christensen-Dalsgaard J., Miesch M. S., Toomre J., 2003, ARA&A, 41, 599
Weber M., Strassmeier K. G., Washuettl A., 2005, Astron. Nachr., 326, 287
Wicht J., 2002, Phys. Earth Planet. Inter., 132, 281
Yadav R. K., Gastine T., Christensen U. R., 2013, Icarus, 225, 185

This paper has been typeset from a TEX/LATEX file prepared by the author.